Article

Synergistic Effects of Topographical Guidance and Electrical Stimulation on Modulation of BMSC Behaviors Using Electrospun Nanofibers Decorated with Nanoscale Protrusions

Yuying Yan [1], Binbin Sun [2], Melissa LD Rayner [3], Yuanfei Wang [1,4], and Tong Wu [1,4,*]

[1] Medical Research Center, The Affiliated Hospital of Qingdao University, Qingdao Medical College, Qingdao University, Qingdao 266000, China
[2] Shanghai Engineering Research Center of Nano-Biomaterials and Regenerative Medicine, College of Biological Science and Medical Engineering, Donghua University, Shanghai 201620, China
[3] Department of Pharmacology, UCL School of Pharmacy, University College London, London WC1N 1AX, UK
[4] Shandong Key Laboratory of Medical and Health Textile Materials, Qingdao University, Qingdao 266071, China
* Correspondence: twu@qdu.edu.cn

Received: 14 April 2026; Revised: 31 May 2026; Accepted: 5 June 2026; Published: 8 June 2026

Abstract: Peripheral nerve injury (PNI) often leads to disability and chronic pain, with limited options available to promote regeneration and functional recovery. Bone marrow mesenchymal stem cells (BMSCs) are considered promising candidates for cell therapy in PNI repair. However, the effective induction of BMSCs towards neurogenesis and the directed migration of cells remain challenging. Here, we constructed a biomimetic environment by combining uniaxially aligned polycaprolactone (PCL) nanofibers containing silica nanoparticles (SiO_2 NPs) with electrical stimulation (ES). A proper portion of SiO_2 NPs was uniformly integrated into uniaxially aligned PCL nanofibers to create nanoscale protrusions on fiber surfaces. Such fibrous mats showed uniaxially aligned morphology, uniform fiber diameter, and improved wettability. BMSCs were then cultured on both the nanofibers with smooth surfaces (PCL) or those decorated with nanoscale protrusions (PCL/SiO_2), followed by treatment with or without ES, with glass slides used as a control. All the fibrous mats showed good cell viability, and the uniaxially aligned fibers induced better cell extension and alignment in comparison to the control group. Both the contact guidance provided by the nanoscale protrusions on fiber surfaces and the biochemical signal from ES contributed to BMSC differentiation, with a combination of both promoting the greatest differentiation into neural-like cells. Immunofluorescence micrographs demonstrated significantly increased expression of NF200 and S100β, along with a higher proportion of NF200-positive cells compared with S100β, indicating the preferred differentiation of BMSCs to neuron-like cells under such conditions. Additionally, in migration assays the greatest number and longest migration distance of BMSCs were exhibited on the PCL/SiO_2 nanofibers with ES. These studies offer valuable strategies for the manipulation of stem cell behavior in PNI repair.

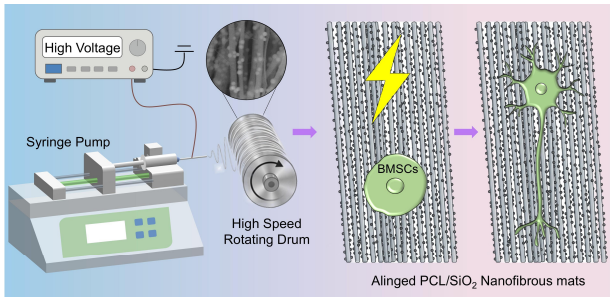

Keywords: bone marrow mesenchymal stem cells; nanofibers; nanoscale protrusions; electrical stimulation; neural differentiation

1. Introduction

Bone marrow mesenchymal stem cells (BMSCs) are regarded as highly promising cell sources for neural tissue engineering owing to their self-renewal capacity, multilineage differentiation potential, relative ease of harvest, and low immunogenicity [1,2]. Under appropriate microenvironmental cues, BMSCs can differentiate toward neural lineages, including neuron-like and Schwann cell-like phenotypes, secrete various neurotrophic factors, and modulate the local immune and inflammatory microenvironment via paracrine signaling [3–5].

However, current strategies for inducing neurogenic differentiation of BMSCs mainly rely on exogenous supplementation of neurotrophic factors or pharmacological agents. These approaches are costly and often associated with suboptimal induction efficiency and limited stability of the differentiated phenotype. Thus, there is a need to develop alternative strategies such as using biophysical and biochemical cues to more effectively direct the fate of BMSCs. Increasing evidence demonstrates that cells can actively sense and respond to biophysical and mechanical factors [6,7]. Biophysical factors are considered one of the most important physical guidance cues that adjust cell behaviors including adhesion, morphology, migration, and differentiation [8–10]. Combined biophysical and biochemical factors have also been widely used to regulate cell behaviors [11–13].

After peripheral nerve injury (PNI), the directional migration of stem cells toward the injury site and their differentiation into neuron-like cells are critical for nerve regeneration and functional recovery [14]. In this regard, constructing a biomimetic microenvironment that integrates both biophysical and biochemical cues represents a key strategy for precisely regulating the adhesion, alignment, migration, and neurogenic differentiation of BMSCs. This approach facilitates the enrichment of both neuron-like and Schwann cell-like phenotypes at the injury site. Among the different types of biomaterials, nanofibrous scaffolds can closely mimic the architecture of native nerve fiber bundles and provide topographical guidance cues for neural cell growth [15]. By adjusting polymer composition and electrospinning parameters, it is possible to modulate fiber orientation, diameter, and surface secondary structures, as well as to introduce biochemical functionalization [16–18]. This enables the construction of engineered nerve regeneration microenvironments that provide multiple physical, chemical, and biological cues to guide neural cell behavior and stem cell differentiation [19,20]. Polycaprolactone (PCL) is a synthetic polymer approved by the U.S. Food and Drug Administration for *in-vivo* implantation. Electrospun PCL fibers often offer excellent biocompatibility, processability, and biodegradability, which have been widely employed in preparing tissue-engineered scaffolds [20,21]. By controlling the collector during the electrospinning process, uniaxially aligned PCL nanofibers can be obtained to mimic the linear arrangement of native nerve fascicles, thereby providing physical guidance for Schwann cell (SCs) migration and facilitating the formation of Büngner bands [22,23]. In addition, neural cells are highly sensitive to the nanoscale topography on fiber surfaces. Our previous study showed that silica nanoparticles (SiO_2 NPs), a commonly used inorganic material with controllable particle size and surface chemistry, can be readily incorporated into electrospun fibers to generate nanoscale protrusions on fiber surfaces and enable further functional modification [24,25]. The introduction of "cell climbing stone-like" structures provided by protrusions on the surfaces of aligned PCL fibers is expected to provide biomimetic cues more closely resembling axonal growth cones, thereby facilitating directed cell migration and axonal extension.

In addition to topographical guidance, external electrical stimulation (ES) usually serves as a clinically relevant and controllable physical modulation strategy, which exhibits clear potential in promoting peripheral nerve regeneration and attenuating muscle atrophy [26,27]. ES can modulate neuronal membrane potentials and ion channel activity, regulate intracellular Ca^{2+} signaling, cAMP levels, and related pathways, thereby promoting axonal sprouting and extension [28–32]. ES also influences SCs proliferation, migration, and the expression of myelin-associated genes, together with promoting a pro-regenerative microenvironment by upregulating neurotrophic factors such as brain-derived neurotrophic factor, nerve growth factor, and glial cell line-derived neurotrophic factor [32–34]. In terms of the modulation of stem cell behaviors, ES shows advantages in regulating stem cell proliferation, migration, and lineage commitment. Several studies have demonstrated the positive effects of ES on lineage-specific differentiation of BMSCs to neural, osteogenic, and chondrogenic lineages [35–38]. Compared with the induction of BMSC differentiation solely based on structural cues, the integration of ES offers temporal controllability, adjustable parameters, and compatibility with nerve conduits, providing an important complement for realizing "structure–function integrated" nerve repair [39]. The combined effects of structural guidance, provided by the aligned nanofibers with nanoscale protrusions, together with the ES treatment on BMSCs neurogenic differentiation and migration, are worth fully elucidating.

In this study, we designed and fabricated SiO_2 NPs-doped PCL (PCL/SiO_2) nanofibrous mats by electrospinning. After systematically characterizing their morphology, wettability, and chemical structure, BMSCs were cultured on the nanofibrous mats, with or without ES, to evaluate cytocompatibility, cell morphology, neurogenic differentiation, and migratory behavior. Neurofilament 200 (NF200) and anti-S100 Beta (S100β) were selected as representative markers of neuronal axons and SCs, respectively, to assess lineage-specific differentiation. By integrating topographical guidance from nanoscale protrusions with ES, this work aims to elucidate the synergistic effects of combined biophysical cues on directing BMSC fate, and to provide a rational design strategy based on cell therapy for PNI repair.

2. Experimental Section

2.1. Materials

Ammonium hydroxide aqueous solution and ethanol absolute were bought from Sinopharm Chemical Reagent Co., Ltd. (Shanghai, China). Tetraethyl orthosilicate (TEOS) and Hexafluoroisopropanol (HFIP) were obtained from Macklin (Shanghai, China). Polycaprolactone (PCL, $M_w = 8 \times 10^4$) and poly-D-lysine (PDL) were supplied by Sigma-Aldrich (Shanghai, China). Electrospinning equipment was bought from Beijing Ucalery Technology and Development Co., Ltd. (Beijing, China). Fetal bovine serum (FBS), low glucose dulbecco's modified eagle medium and phosphate-buffered saline (PBS) were procured from Wuhan Procell Biotechnology Co., Ltd. (Wuhan, China). Specialized growth media design for mesenchymal stem cells was procured by Xirui Infinity Biotechnology Co., Ltd. (Hangzhou, China). Penicillin-Streptomycin Solution was obtained from Biosharp (Beijing, China). 4% paraformaldehyde, mounting medium, antifade (with DAPI), Triton X-100, and bovine serum albumin (BSA) were purchased from Beijing Solarbio Science & Technology Co., Ltd. (Beijing, China). Phalloidin-iFluor 488 was bought from Abcam (Cambridge, UK). Osteogenic, adipogenic, and chondrogenic differentiation kits were purchased from Haixing Biosciences (Jiangsu, China). NF200 Polyclonal antibody (NF200) and anti-S100 Beta Monoclonal antibody (S100β) were procured from Proteintech (Wuhan, China).

2.2. Preparation of PCL/SiO_2 Nanofibrous Mats

The Stöber process was used to synthesize SiO_2 NPs [40,41]. Briefly, 5 mL of ammonium hydroxide aqueous solution and 12 mL of deionized water were added to a beaker and stirred using a magnetic stirrer for 10 min to obtain stock solution A. Stock solution B was prepared by mixing 3 mL TEOS and 47 mL absolute ethanol. Stock solutions A and B were then mixed uniformly, and the reaction was allowed to proceed at room temperature for 2 h. Subsequently, the SiO_2 NPs were obtained by centrifugation, washing, and subsequent drying. The morphology of the particles was analyzed using a scanning electron microscope (Regulus8100, Hitachi, Tokyo, Japan). The SiO_2 NPs were then investigated by dynamic light scattering (DLS) in triplicate (90Plus PALS, Brookhaven Instruments Corporation, New York, USA).

According to our previous study, a dispersion of SiO_2 NPs with concentrations of 6% (*w*/*v*) was prepared by ultrasonication in HFIP for 2 h uniformly [24]. PCL was dissolved in suspension to formulate an electrospinning solution with a final concentration of 10 wt%. The prepared PCL/SiO_2 aligned nanofibers were fabricated by electrospinning, with a high-speed rotating drum employed as the collector. The electrospinning parameters used included an applied voltage of 15 kV, collection distance of 18 cm, and rotating speed of the drum at 3000 rpm. The morphology of the fibers was analyzed by the scanning electron microscope. The distribution of SiO_2 NPs within the fibers was observed using a transmission electron microscope (TEM) (HT7700, Hitachi, Tokyo, Japan). Fourier transform infrared spectroscopy (FTIR) (Nicolet iS50, Thermo Fisher Scientific, Waltham, MA, USA) was used to evaluate whether SiO_2 NPs were successfully encapsulated. The hydrophilicity and hydrophobicity of the nanofibrous mats were measured at room temperature using a contact angle analyzer (Theta Lite, Biolin Scientific, Gothenburg, Sweden).

2.3. In Vitro Experiments

Different samples were placed in 24-well or 6-well plates and subjected to plasma sputtering for 30 s, followed by sterilization with 75% ethanol for 4 h and subsequent UV irradiation for 30 min. The samples were then coated with PDL overnight. After removing the PDL, the samples in each well were rinsed with PBS three times. Direct current ES was used in this study at 0.14 mA for 15 min, once daily. The designated experimental groups were as follows: Control (C), Control with ES (CE), PCL (P), PCL with ES (PE), PCL/SiO_2 (S), and PCL/SiO_2 with ES (SE).

2.3.1. Characterization of BMSCs

Morphological Observation: BMSCs at passage 3 (P3) were cultured in specialized growth media. When the cells reached approximately 80–90% confluence, their morphology was examined and photographed under an inverted light microscope.

Osteogenic differentiation: BMSCs at P3 were seeded at 4×10^4 cells/well in 24-well plates. When the cells reached approximately 90–100% confluence, the medium was replaced with osteogenic induction medium and cultured for 21 days, with the medium changed every 3 days. After fixation with 4% paraformaldehyde, mineralized nodules were stained with Alizarin Red S solution for 5 min at room temperature and observed under a light microscope.

Adipogenic differentiation: BMSCs at P3 were seeded at 4×10^4 cells/well in 24-well plates. When the cells reached approximately 80–90% confluence, adipogenic induction medium was added. After 3 days, the medium was changed to adipogenic maintenance medium for 1 day, followed by another 3-day induction cycle. This cycle was repeated for 14 days. Cells were fixed with 4% paraformaldehyde for 30 min and stained with Oil Red O working solution (stock:saline = 3:2) for 30 min.

Chondrogenic differentiation: BMSCs at P3 were seeded at 4×10^5 cells/well in 24-well plates. After 3 h of attachment, 200 μL of medium was added. The cells were cultured for 14 days with medium changes every 3 days. Cells were fixed with 4% paraformaldehyde for 30 min, then stained with Alcian Blue solution for 30 min in the dark. All staining results were observed under an inverted light microscope.

2.3.2. Cell Viability

The CCK-8 assay was used to assess the biocompatibility of various nanofibrous mats with or without ES after 3 and 7 days. Low glucose Dulbecco's modified eagle medium supplemented with 1% (v/v) penicillin-streptomycin solution and 10% (v/v) FBS was used to culture BMSCs. BMSCs were co-cultured with the different material groups in 24-well plates with 2×10^4 cells/well. After cell attachment, ES was applied, and the absorbance of the supernatant was measured at 450 nm by a microplate reader (FLUOstar Omega, BMG Labtech, Offenburg, Germany).

2.3.3. Cell Morphology

BMSCs were seeded into 24-well plates with 1×10^4 cells/well in 400 μL of specialized growth media. After cell adhesion, ES was applied. The media was changed every other day, and ES was continuously applied for 3 days. After the media was removed, cells were fixed with 4% paraformaldehyde for 20 min, permeabilized with 0.1% Triton X-100 for 5 min, and blocked with 1% BSA for 1 h. The cells were then stained with Phalloidin-iFluor 488 followed by antifade (with DAPI) and imaged on an inverted fluorescence microscope.

2.3.4. Cell Differentiation

BMSCs were seeded into the 24-well plates at a density of 5×10^3 cells/well in 400 μL of specialized growth media. After cell adhesion, ES was applied continuously for 7 days, and the media was changed every other day. At 7 days post seeding, the samples were fixed, permeabilized, and blocked following the same protocol as described in Section 2.3.2. Cells were subsequently stained with NF200, S100β, and antifade (with DAPI), respectively, for observation. ImageJ software was used to quantify the fluorescence intensity of NF200 and S100β. Briefly, fluorescence images were imported into ImageJ, and identical thresholding and analysis settings were applied to all groups. Regions of interest (ROIs) were defined for each image, the mean fluorescence intensity was measured after background subtraction, and the values of experimental groups were normalized to the average intensity of the control group. $I_{sample,i}$ is the mean fluorescence intensity of an individual experimental group sample, $I_{control,mean}$ is the average intensity of all control samples, and n is the number of experimental samples. This calculation gives the mean relative intensity normalized to the control group. The relative fluorescence intensity was calculated by normalizing the mean fluorescence intensity of each sample to the average fluorescence intensity of the control group, according to the following formula, as well as the proportion of differentiated cells. The proportion of differentiated cells (NF200-positive or S100β-positive cells) was calculated.

$$\text{Relative intensity} = \frac{1}{n}\sum_{i=1}^{n}\frac{I_{sample,i}}{I_{control,mean}}$$

2.3.5. Cell Migration

PCL and PCL/SiO_2 fibrous mats were placed in 6-well plates, respectively, with glass slides as a control. BMSCs were seeded at a density of 1×10^5 cells/well on the left side of each sample with a 0.3-mm wide area produced using a polydimethylsiloxane (PDMS) block. After the cells had adhered to the substrate, the PDMS block was removed to allow the migration of cells into a region of 1 cm, and the media was replaced with specialized growth media to low-glucose DMEM containing 1% FBS. At 3 days post seeding and daily ES, the cells were fixed, permeabilized, blocked, and stained with Phalloidin-iFluor 488 and antifade (with DAPI) following the same procedure as described in Section 2.3.2. The micrographs were captured under the inverted fluorescence microscope, and the total number of migrated cells as well as the cell counts in each migration region were quantified using the ImageJ software.

2.4. Statistical Analysis

All experiments in this study were conducted with at least three replicates. All data were processed and analyzed using GraphPad Prism 10.1.2 (GraphPad Software, San Diego, CA, USA) and ImageJ (National Institutes of Health, Bethesda, MD, USA), and results were presented as mean ± standard deviation (SD). Student's *t*-test was used for comparisons between two groups only. For experiments involving the six groups C, CE, P, PE, S, and SE and two independent variables, a two-way ANOVA was applied. Statistical significance is presented as follows: * $p < 0.05$, ** $p < 0.01$ and *** $p < 0.001$.

3. Results and Discussion

3.1. Characterization of SiO_2 NPs and PCL/SiO_2 Nanofibrous Mats

SiO_2 NPs were synthesized via the Stöber method. The scanning electron microscopy (SEM) images in Figure 1A show that the SiO_2 NPs have smooth surfaces, good dispersibility, and a uniform size distribution around 200 nm. DLS analysis in Figure 1E shows that the hydrodynamic diameter of the SiO_2 NPs was 241.29 ± 21.87 nm. This discrepancy arises because DLS measures the hydrodynamic diameter of particles in solution, including the hydration layer surrounding the nanoparticles, whereas SEM images show the physical diameter of dry particles under vacuum. Such differences are commonly observed in nanoparticle characterization. Our previous study demonstrated that PCL microfibers engraved with nanoscale grooves around 200 nm showed the best performance in inducing neurite extension and SCs migration [42]. Additionally, we integrated SiO_2 NPs with biocompatible PCL to fabricate hybrid nanofibers featuring surface protrusions as secondary structures with distinct sizes and SiO_2 concentrations [24]. The results also confirmed that the SiO_2 NPs with a diameter of around 200 nm demonstrated the most obvious influence on the migration of SCs and neural stem cells and contributed to the axonal extension of neurons. These results are mainly attributed to the modulation of surface roughness and hydrophilicity of SiO_2 NPs, which may enhance cell adhesion and cytoskeletal remodeling. Meanwhile, 200 nm protrusions match the dimension of growth cones, thereby reinforcing cell–material interactions and amplifying guidance effects.

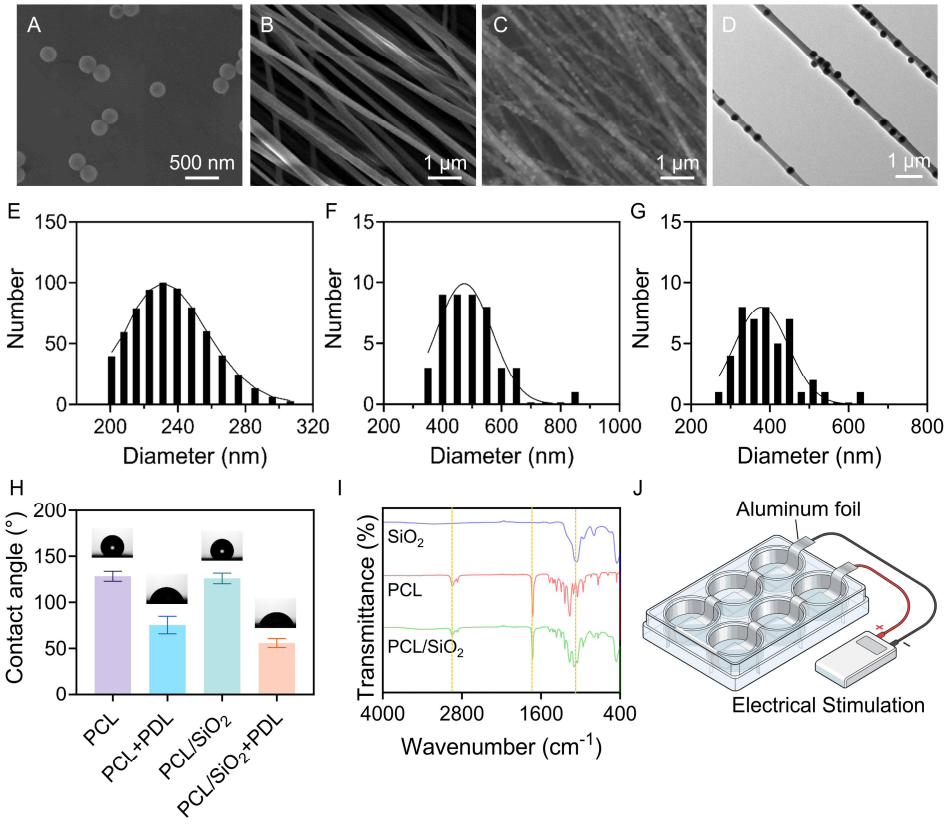

Figure 1. SEM images of (**A**) SiO_2 NPs, (**B**) PCL nanofibers, and (**C**) PCL/SiO_2 nanofibers. (**D**) TEM image of PCL/SiO_2 nanofibers. (**E**) Size distribution of SiO_2 NPs measured by DLS. Diameter distribution of (**F**) PCL and (**G**) PCL/SiO_2 nanofibers. (**H**) Water contact angle analysis. (**I**) FTIR spectra of SiO_2 NPs, PCL and PCL/SiO_2 nanofibers. (**J**) Schematic illustration of the electrical stimulation system used for in vitro cell stimulation.

Aligned PCL and PCL/SiO_2 nanofiber mats were successfully fabricated by electrospinning. SEM observations in Figures 1B and 1C confirm the morphologies of PCL and PCL/SiO_2 nanofibers, which were uniformly distributed and exhibited a predominantly aligned morphology, as observed by SEM. Such fibers are known to provide contact guidance cues for cell alignment and migration [24]. TEM analysis in Figure 1D presents that SiO_2 NPs are distributed along the PCL nanofibers, showing both surface-decorated and embedded morphologies. Although the present study did not quantitatively determine the density, height, or spatial distribution of the nanoscale protrusions by AFM or profilometry, SEM and TEM observations confirmed the aligned fibrous morphology and the presence of SiO_2 nanoparticle-derived surface features. The particle dispersion and aggregation state are expected to strongly influence the surface properties of composite fibers. Statistical analysis in Figures 1F and 1G showed that the average fiber diameter of PCL mats was 496.33 ± 96.1 nm, whereas that of PCL/SiO_2 mats decreased to 394.58 ± 71.1 nm. The incorporation of SiO_2 NPs affected the electrospinning process and resulted in a narrower diameter distribution. The decrease in fibrous diameter can be explained by the typical parameters for electrospinning and the polymer composition [43,44]. When SiO_2 NPs are added to the solution for electrospinning, the NPs significantly improve the conductivity and charge density, resulting in stronger stretching forces and enhanced whipping instability of the jet in the electric field, thereby enabling the fibers to be drawn thinner before solidification. Moreover, the SiO_2 NPs could influence the surface tension or increase the electrostatic interaction between the solution and the collector.

Wettability plays a critical role in regulating cell adhesion and spreading [45]. The water contact angles of PCL and PCL/SiO_2 nanofiber mats were 128.34 ± 4.93° and 126.02 ± 5.2°, respectively (Figure 1H). Plasma was then applied to treat the nanofiber mats, followed by coating with PDL. The contact angle was markedly decreased to 75.39 ± 8.66° and 55.92 ± 4.42°, respectively. The improved wettability is likely related to the surface activation effect of plasma treatment. Plasma exposure may cause mild surface etching and generate nanoscale irregularities, potentially increasing the apparent surface roughness. Meanwhile, plasma treatment introduces oxygen-containing polar groups, such as hydroxyl (-OH), carbonyl (C=O), and carboxyl (-COOH), onto polymer surfaces. These changes are expected to enhance surface energy and facilitate subsequent PDL deposition, thereby promoting cell adhesion and migration. The chemical structures of SiO_2 NPs, PCL and PCL/SiO_2 nanofibers were characterized by FTIR, as shown in Figure 1I. For the PCL/SiO_2 nanofibers, a characteristic absorption band at 1710 cm^{-1} was observed, corresponding to the C=O stretching vibration of PCL. Moreover, the peaks at approximately 2940 cm^{-1} ascribed to C–H stretching were enhanced after the incorporation of SiO_2 NPs [46]. The appearance of bands around 765 cm^{-1} in the PCL/SiO_2 spectrum was assigned to the Si–O stretching vibration of SiO_2 [47], demonstrating the successful incorporation of SiO_2 NPs into the PCL fibers.

3.2. Characterization of BMSCs

The isolated and cultured cells exhibited typical mesenchymal stem cell morphology, as shown in Figure S1, with adherent growth and a spindle-shaped or fibroblast-like appearance under an inverted microscope. To further identify their stem cell characteristics, trilineage differentiation assays were performed. After osteogenic induction, Alizarin Red S staining showed distinct red-stained mineralized nodules, indicating calcium deposition and osteogenic differentiation potential (Figure S2). Following chondrogenic induction, positive Alcian blue staining was observed, demonstrating the accumulation of acidic glycosaminoglycans in the extracellular matrix and confirming chondrogenic differentiation ability (Figure S3). After adipogenic induction, Oil Red O staining revealed abundant intracellular lipid droplets, and Figure S4 indicates adipogenic differentiation potential. Together, these results confirmed that the cells used in this study possessed the typical morphological features and multilineage differentiation capacity of BMSCs.

3.3. In Vitro Biocompatibility Evaluation

As shown in Figure 1J, an in vitro electrical stimulation system was constructed for subsequent cell experiments. Aluminum foil was used as the electrode material, integrated into a culture plate, and connected to an external ES. This simple setup allowed electrical cues to be applied during cell culture and served as the basis for evaluating the synergistic effects of topography and electrical stimulation on BMSC behaviors.

To evaluate the biocompatibility of the topographical nanofibrous mats combined with ES, BMSCs cultured on the different substrates were evaluated using the CCK-8 assay at days 3 and 7. As shown in Figure 2, there are no statistically significant differences in overall BMSCs viability, indicating that the aligned PCL/SiO_2 nanofibers, with or without ES, exhibit good cytocompatibility and support BMSCs growth. Fluorescent micrographs in Figure 3A present the morphologies of BMSCs after culture in the different groups for 3 days. In the control group (C), BMSCs displayed a typical fibroblast-like morphology with a relatively spread and polygonal shape. With the

introduction of aligned fibers and ES, cells gradually became more elongated and aligned along the fiber direction. As shown in Figure 3B, the orientation angle of BMSCs was widely distributed in the C group, indicating no obvious directional preference. In contrast, the aligned fibrous mat groups exhibited a narrow angular distribution, with a larger proportion of cells oriented close to the fiber direction. These data demonstrate that aligned fibers play a major role in guiding BMSCs' orientation, while ES can further improve the degree of ordered cell arrangement. This morphological transition implies that the combined physical guidance of fiber orientation and ES may induce a neurogenic-like response in BMSCs. Such morphological changes are often associated with cytoskeletal rearrangement and may represent an early indicator of lineage commitment toward neural phenotypes. Therefore, the synergistic effects of topographical guidance and electrical cues appear to modulate BMSCs' morphology and potentially prime cells for neurogenic differentiation.

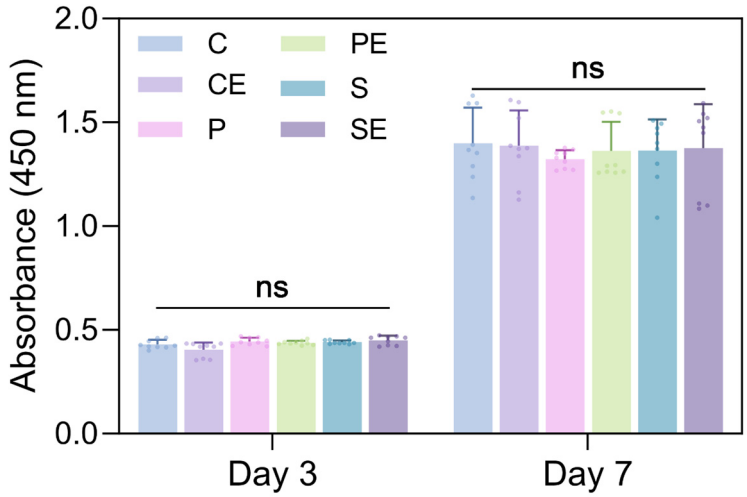

Figure 2. Viability of BMSCs after culture in the different groups for 3 and 7 days. The experimental groups were designed as follows: control (C), control with ES (CE), PCL (P), PCL with ES (PE), PCL/SiO_2 (S), and PCL/SiO_2 with ES (SE). ns indicates no significant differences between the compared groups.

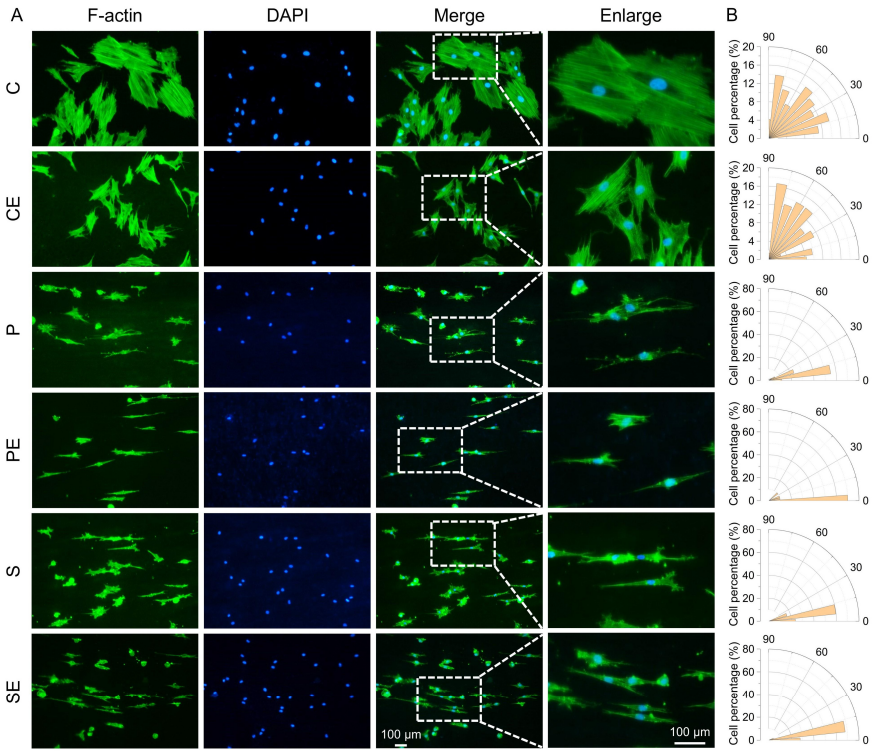

Figure 3. (**A**) The morphology of BMSCs after culture on the different groups for 3 days; (**B**) Orientation angles of BMSCs on the different groups. F-actin (green) represents the cytoskeleton and DAPI (blue) is a nuclei stain. The experimental groups were designed as follows: control (C), control with ES (CE), PCL (P), PCL with ES (PE), PCL/SiO_2 (S), and PCL/SiO_2 with ES (SE).

3.4. Differentiation of BMSCs

Following PNI, remyelination and axonal extension are two critical biological steps for functional regeneration [48]. The myelin sheath is an insulating structure formed by SCs that wraps around the axons [49]. It not only enables saltatory conduction of action potentials but also provides neurotrophic support to the axon [50,51]. Axons, as the extending part of the neuron, are responsible for conducting nerve impulses and serve as the foundation for establishing functional neural connections [52]. Therefore, simultaneously promoting axonal regeneration and remyelination is the goal of neural tissue engineering. NF200, as a structural protein in neurons, implies the growth of nerve fibers, while S100β serves as a cytoplasmic protein marker for SCs. To investigate the regulatory effects of topographical cues combined with ES on neural-like differentiation of BMSCs, the expression of NF200 and S100β was assessed by immunofluorescence. With the introduction of aligned fibers and ES, consistent with the morphological observations, BMSCs demonstrated elongated cell morphology and aligned growth and expressed both NF200 and S100β (Figure 4).

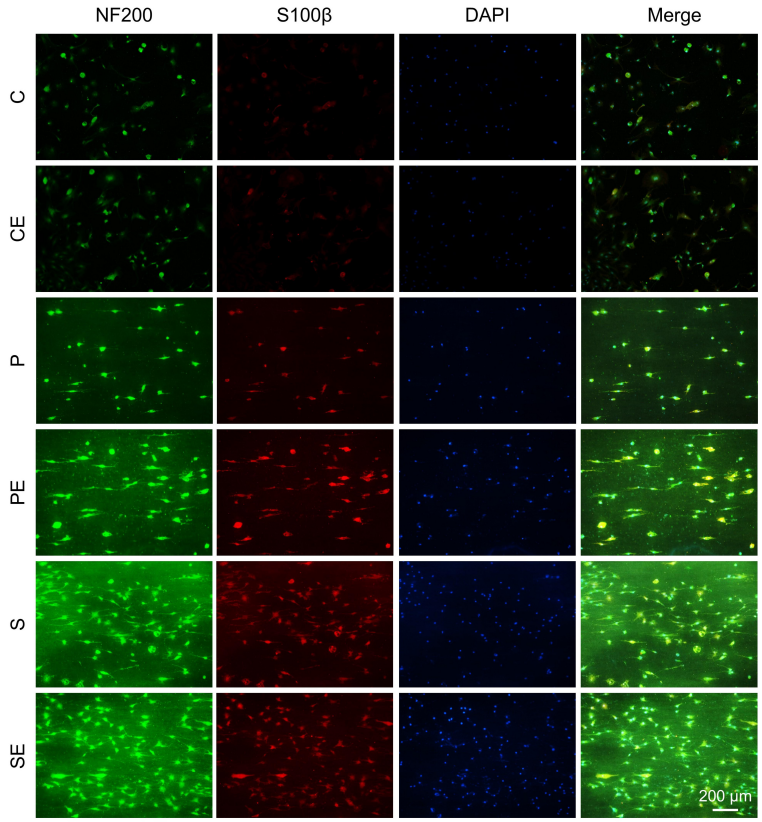

Figure 4. Immunofluorescence micrographs showing NF200 and S100β expression after BMSCs were cultured on the different groups for 7 days. Green: NF200; Red: S100β; Blue: DAPI nuclei stain. The experimental groups were designed as follows: control (C), control with ES (CE), PCL (P), PCL with ES (PE), PCL/SiO_2 (S), and PCL/SiO_2 with ES (SE).

Quantitative analysis of fluorescence intensity in Figures 5A and 5B revealed that both the nanoscale protrusions on fiber surfaces and the ES contributed to the induction of BMSCs differentiation, with the highest NF200 and S100β expression seen in the SE group. Compared to the C group, aligned PCL nanofibers (P group) also induced a significant upregulation of NF200 expression. Incorporation of SiO_2 NPs in aligned PCL nanofibers (S group) further enhanced NF200 expression compared with the C group, indicating that nanoscale protrusions augment the physical guidance effect of fiber alignment. The expression of NF200 was significantly higher in the groups exposed to ES compared to those without, particularly in the SE group. On the other hand, BMSCs exposed to both nanoscale protrusions and ES showed the highest Schwann cell-like differentiation in comparison to the other groups, suggesting beneficial synergistic effects of physical and biochemical signals. These results suggest that the integration of nanoscale topography with ES effectively enhances the neural-like differentiation of BMSCs. Notably, compared with nanoscale protrusions, ES more effectively induced differentiation into Schwann cell-like cells. Overall, aligned fibers with nanoscale protrusions on fiber surfaces offered a structure similar to Büngner bands, which provided guidance for cell elongation. Additionally, ES could regulate the level of Ca^{2+} and activate downstream pathways, which played a significant role in regulating axonal extension. The synergistic

effects may stem from the elongation of cell morphology introduced by nanoscale protrusions on aligned fiber surfaces, which enhances the sensitivity to ES, thereby enlarging neuronal signaling.

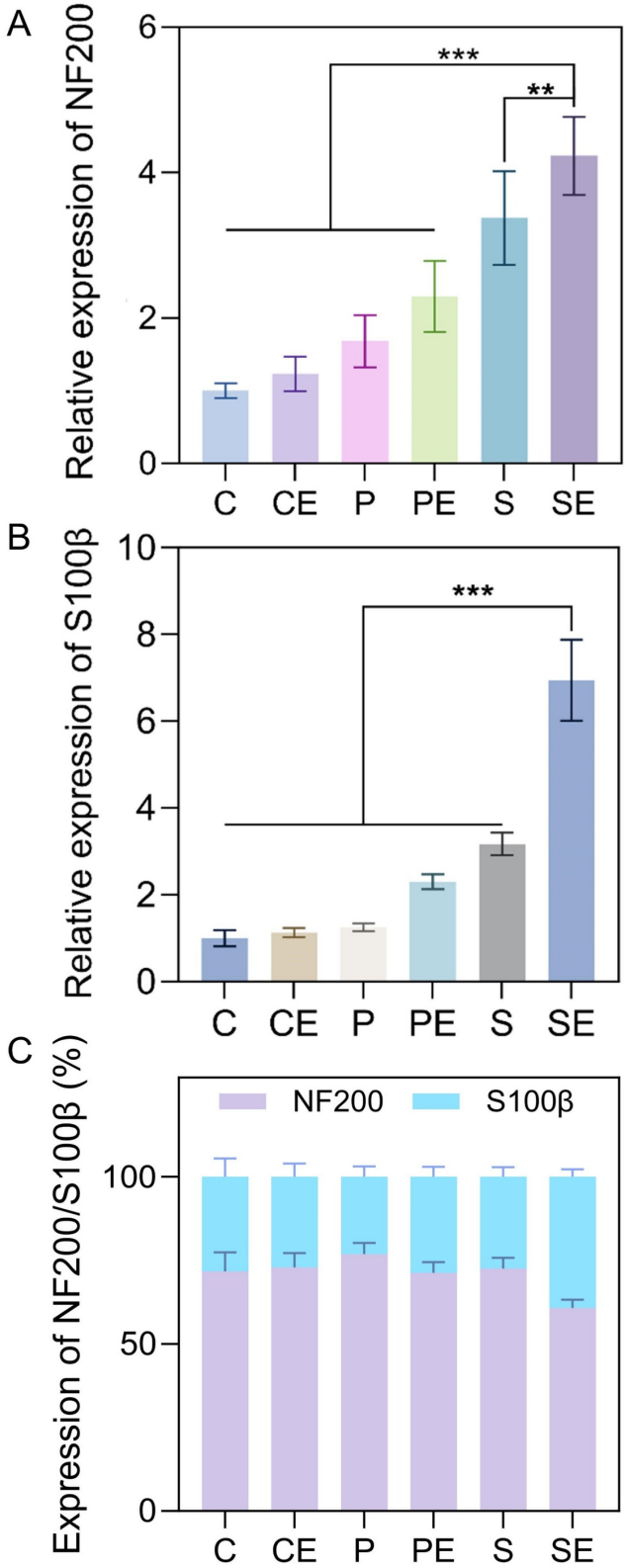

Figure 5. Relative expression of NF200 and S100β proteins according to the results shown in Figure 4: (**A**) NF200; (**B**) S100β; (**C**) Comparison of NF200/S100β expression. The experimental groups were designed as follows: control (C), control with ES (CE), PCL (P), PCL with ES (PE), PCL/SiO_2 (S), and PCL/SiO_2 with ES (SE). ** $p <$ 0.01 and *** $p < 0.001$ indicate significant differences between the compared groups.

Moreover, data showed that the proportion of cells expressing NF200 was higher than that expressing S100β in each group, as presented in Figure 5C. Aligned PCL nanofibers induced a significant increase in NF200 relative

to the C group and altered the NF200/S100β ratio in a direction consistent with a more neuron-like phenotype. Following the application of ES, the expression level of NF200 exhibited a slight decrease. Nevertheless, it remained significantly elevated compared with that of S100β. These results indicate a preference for neuronal-like differentiation rather than Schwann cell-like differentiation under these conditions. The synergy between the nanoscale topography of SiO_2-containing aligned fibers and ES can effectively promote the neurogenic differentiation of BMSCs, with a bias toward a neuron-like phenotype.

3.5. Migration of BMSCs

Cell migration is a critical process during nerve regeneration, as stem cells must migrate toward injury sites and participate in tissue repair [53]. We further evaluated the influence of PCL/SiO_2 fibers combined with ES on the migration of BMSCs. Fluorescence micrographs in Figure 6A showed that BMSCs in all groups exhibited migration behaviors on the underlying substrates. Compared to the C group, the migration of BMSCs on uniaxially aligned fibers (P, PE, S, and SE) displayed substantially enhanced migration, characterized by a longer migrated distance. This result indicates that the aligned fiber architecture provided effective contact-guidance cues to facilitate directional cell movement. Furthermore, the BMSCs cultured on fiber surfaces with nanoscale protrusions (S group) exhibited a more significant response to directional migration, compared to the smooth nanofibers (P group). When combined with ES, the BMSCs migrated the farthest distance in the SE group. Quantitative statistical analysis in Figure 6B further revealed that the total number of migrated cells in the SE group was significantly greater than that in the other groups (*** $p < 0.001$), suggesting a synergistic contribution of biomimetic nano-topography and ES in enhancing BMSCs migration. To further evaluate migration distribution, the migration zone was evenly divided into three regions: the proximal (region I), middle (region II), and distal area (region III) in Figure 6C. In regions I and II, the number of migrated BMSCs in the SE group was significantly greater (*** $p < 0.001$) than in the C and CE groups. Even in region III, the SE group exhibited a significantly higher number of migrated cells (* $p < 0.05$) than the C and CE groups. These results revealed that the combination of biophysical and biochemical cues enabled BMSCs to migrate over longer distances.

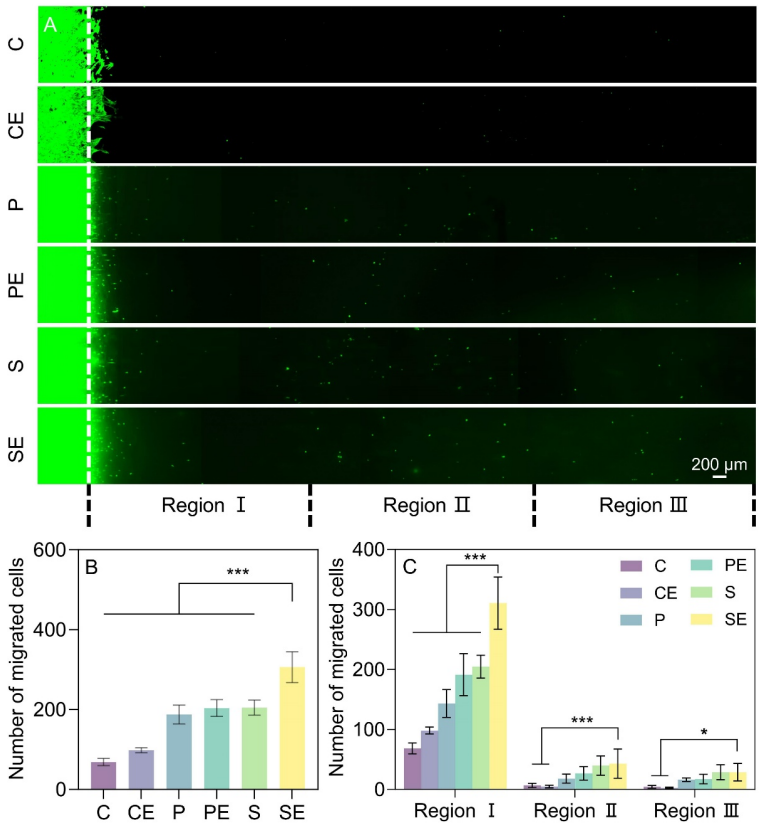

Figure 6. (**A**) Fluorescence micrographs showing the migration of BMSCs after culture on the different groups for 3 days. (**B**) Statistics of the total number of migrated BMSCs. (**C**) The number of BMSCs in the different migration zones. The experimental groups were designed as follows: control (C), control with ES (CE), PCL (P), PCL with ES (PE), PCL/SiO_2 (S), and PCL/SiO_2 with ES (SE). * $p < 0.05$ and *** $p < 0.001$ indicate significant differences between the compared groups.

Uniaxially aligned nanofibers with nanoscale protrusions offer more anchoring sites to reduce the randomness of cell movement and improve migration efficiency. Such nano-topographical features may also enhance signaling related to cell migration, such as the reaction of actin mediated by Rho, Rac, and Cdc42 GTPases, and actin remodeling [54]. Meanwhile, ES served as an external bioelectrical cue that further enhanced directional migration, possibly by modulating membrane potential, ion channel activity, and intracellular calcium dynamics, thereby accelerating cell movement and improving directional persistence. More importantly, the simultaneous presence of topographical and electrical cues may create a more biomimetic microenvironment, enabling BMSCs to integrate multiple external signals and respond more sensitively to guidance stimulation [55]. This cooperative effect likely underlies the superior migration performance observed in the SE group and may be particularly beneficial for promoting endogenous stem cell recruitment and tissue regeneration in peripheral nerve repair.

4. Conclusions

By utilizing electrospinning, SiO_2 NPs were integrated with biocompatible PCL to fabricate hybrid nanofibers featuring surface protrusions as secondary structures. We explored the regulatory influence of PCL/SiO_2 nanofibrous mats combined with ES on modulating BMSCs' behavior. Our results demonstrated that the fabricated scaffolds possessed favorable physicochemical properties and cytocompatibility, effectively promoting cell adhesion, migration, and viability. The synergistic effect of the uniaxially aligned topographical structure and applied ES induced a neural-like morphological transition of BMSCs. In particular, this combined approach significantly upregulated the neuronal marker NF200 and the Schwann cell marker S100β, with a bias toward neuronal-like differentiation. The uniaxially aligned PCL/SiO_2 nanofibers combined with ES also markedly enhanced the long-distance migration of BMSCs. Collectively, these findings indicate that the combination of aligned PCL/SiO_2 nanofibrous scaffolds with ES creates a biomimetic microenvironment that resembles native neural tissue architecture. Furthermore, it is indicated that fibrous mats seeded with stem cells to create nerve guidance conduits represent a significant potential for future applications in PNI repair.

Supplementary Materials: The following supporting information can be downloaded at: https://media.sciltp.com/articles/others/2606081418394895/MI-26040102-SI.pdf, Figure S1: Representative light microscopy image showing the typical spindle-shaped and fibroblast-like morphology of cultured BMSCs; Figure S2: Alizarin Red S staining showing BMSCs formed mineralized nodes under osteogenic induction, showing the formation of mineralized nodules; Figure S3: Alcian blue staining after chondrogenic induction, showing the deposition of cartilage-associated extracellular matrix; Figure S4: Oil Red O staining after adipogenic induction, showing the formation of intracellular lipid droplets.

Author Contributions: Y.Y.: Investigation, Methodology, Visualization, Writing—original draft; B.S.: Methodology; M.L.R.: Writing—review & editing; Y.W.: Supervision, Resources; T.W.: Conceptualization, Supervision, Resources, Funding acquisition, Writing—review & editing. All authors have read and agreed to the published version of the manuscript.

Funding: This work was supported by the Young Scientist Project of National Key R&D Program of China (2025YFC2426600), Natural Science Foundation of Shandong Province (ZR2024JQ026), and National Natural Science Foundation of China (12411530081).

Data Availability Statement: The data that support the findings of this study are available from the corresponding author upon reasonable request.

Acknowledgments: The authors also gratefully acknowledge the support provided by the Youth Science and Technology Innovation Team of the Shandong Provincial Health Commission.

Conflicts of Interest: The authors declare no conflict of interest.

Use of AI and AI-Assisted Technologies: No AI tools were utilized for this paper.

References

1. Ahmad, P.; Estrin, N.; Farshidfar, N.; Zhang, Y.; Miron, R. Isolation methods of exosomes derived from dental stem cells. *Int. J. Oral Sci.* **2025**, *17*, 846–855.
2. Chen, L.; He, D.; Zhang, Y. Differentiation of mesenchymal stem cells from rat bone marrow into dopaminergic neuron-like cells in vitro. *Blood* **2007**, *110*, 4067.
3. Wei, Z.; Fan, B.; Liu, Y.; Ding, H.; Tang, H.; Pan, D.; Shi, J.; Zheng, P.; Shi, H.; Wu, H.; et al. MicroRNA changes of bone marrow-derived mesenchymal stem cells differentiated into neuronal-like cells by schwann cell-conditioned medium. *Neural Regen. Res.* **2019**, *14*, 1462–1469.
4. Simsar, E.; Cheng, P.; Dogruel, T.; Donta, M.; Jung, J.; Asante, N.; Sakaguchi, D.; Mallapragada, S.; Kidambi, P.; Metin, U. Few-layered conductive graphene foams for electrical transdifferentiation of mesenchymal stem cells into schwann cell-like phenotypes. *Adv. Healthc. Mater.* **2026**, *15*, e02204.

5. Li, J.; Zhang, D.; Guo, S.; Zhao, C.; Wang, L.; Ma, S.; Guan, F.; Yao, M. Dual-enzymatically cross-linked gelatin hydrogel promotes neural differentiation and neurotrophin secretion of bone marrow-derived mesenchymal stem cells for treatment of moderate traumatic brain injury. *Int. J. Biol. Macromol.* **2021**, *187*, 200–213.
6. Wan, X.; Liu, Z.; Li, L. Manipulation of stem cells fates: The master and multifaceted roles of biophysical cues of biomaterials. *Adv. Funct. Mater.* **2021**, *31*, 2010626.
7. Liu, N.; Ning, X.; Zhang, X.; Zhou, Z.; Fu, M.; Wang, Y.; Wu, T. Gradient galectin-1 coating technology: Bionic multichannel nerve guidance conduits promote neural cell migration. *Adv. Technol. Neurosci.* **2024**, *1*, 276–289.
8. Sousa, M.; Arab-Tehrany, E.; Cleymand, F.; Mano, J. Surface micro- and nanoengineering: Applications of layer-by-layer technology as a versatile tool to control cellular behavior. *Small* **2019**, *15*, e1901228.
9. Zhang, X.; Guo, M.; Guo, Q.; Liu, N.; Wang, Y.; Wu, T. Modulating axonal growth and neural stem cell migration with the use of uniaxially aligned nanofiber yarns welded with NGF-loaded microparticles. *Mater. Today Adv.* **2023**, *17*, 100343.
10. Chen, R.; Wang, Y.; Yu, C.; Zhang, X.; Wang, Y.; Yu, T.; Wu, T. Bioactive glass-reinforced hybrid microfibrous spheres promote bone defect repair via stem cell delivery. *Adv. Funct. Mater.* **2025**, *7*, 240–253.
11. Xue, J.; Wu, T.; Li, J.; Zhu, C.; Xia, Y. Promoting the outgrowth of neurites on electrospun microfibers by functionalization with electrosprayed microparticles of fatty acids. *Angew. Chem. Int. Ed. Engl.* **2019**, *58*, 3948–3951.
12. Li, Z.; Zhou, Y.; Li, T.; Zhang, J.; Tian, H. Stimuli-responsive hydrogels: Fabrication and biomedical applications. *Biomater. Sci.* **2022**, *3*, 20200112.
13. Yao, L.; Yan, Y.; Zhang, H.; Zhang, X.; Lan, J.; Chen, Y.; Rayner, M.; Wang, Y.; Wu, T. Engineered nanofiber-based nerve guidance conduit facilitates the restoration of peripheral nerve injury through enhanced vascularization. *Small* **2026**, *22*, e14312.
14. Wei, S.; Xiong, F.; Gu, H.; Zhang, Z.; Xuan, H.; Jin, Y.; Xue, Y.; Li, B.; Feng, W.; Yuan, H. Highly aligned electroactive ultrafine fibers promote the differentiation of mesenchymal stem cells into schwann-like cells for nerve regeneration. *Int. J. Biol. Macromol.* **2024**, *279*, 135388.
15. Wu, J.; Hong, Y. Enhancing cell infiltration of electrospun fibrous scaffolds in tissue regeneration. *Bioact. Mater.* **2016**, *1*, 56–64.
16. Xue, J.; Xie, J.; Liu, W.; Xia, Y. Electrospun nanofibers: New concepts, materials, and applications. *Acc. Chem. Res.* **2017**, *50*, 1976–1987.
17. Fang, J.; Nan, L.; Song, K.; Weng, Z.; Shan, J.; Shahin, V.; Liu, J.; Qian, Y. Application and progress of bionic scaffolds in nerve repair: A narrative review. *Adv. Technol. Neurosci.* **2024**, *1*, 43–50.
18. Wang, J.; Zhou, Z.; Zhang, X.; Fu, M.; Fang, K.; Wang, Y.; Wu, T. One-Step manufacture and crosslinking of gelatin/polygonum sibiricum polysaccharide bioactive nanofibrous sponges for rapid hemostasis and infected wound healing. *Adv. Fiber Mater.* **2025**, *7*, 1148–1164.
19. Chen, S.; Zhang, X.; Guo, Q.; Yan, Y.; Fu, M.; Wang, Y.; Wu, T. Complex bioactive nanofibrous dura mater repairs traumatic brain injury. *Neural Regen. Res.* **2026**, *21*, 4275–4289.
20. Chaudry, A.; Wu, J.; Wang, H.; Mo, X.; Bhutto, M.; Sun, B. Research and application of conductive nanofiber nerve guidance conduits for peripheral nerve regeneration: A narrative review. *Adv. Technol. Neurosci.* **2025**, *2*, 47–57.
21. Dethe, M.; Prabakaran, A.; Ahmed, H.; Agrawal, M.; Roy, U.; Alexander, A. PCL-PEG copolymer based injectable thermosensitive hydrogels. *J. Control. Release* **2022**, *343*, 217–236.
22. Wang, X.; Chen, S.; Chen, X.; Wu, J.; Huang, Z.; Wang, J.; Chen, F.; Liu, C. Biomimetic multi-channel nerve conduits with micro/nanostructures for rapid nerve repair. *Bioact. Mater.* **2024**, *41*, 577–596.
23. Wang, H.; Zhang, P.; Lu, P.; Cai, X.; Wang, G.; Xu, X.; Liu, Y.; Huang, T.; Li, M.; Qian, T.; et al. Neural tissue-engineered prevascularization in vivo enhances peripheral neuroregeneration via rapid vascular inosculation. *Mater. Today Bio.* **2023**, *21*, 100718.
24. Wang, Y.; Zhang, X.; Yao, L.; Yan, Y.; Wang, Y.; Wu, T. "Cell climbing stones"-varying the surfaces of electrospun nanofibers with protrusions as secondary structures to manipulate neural cell behaviors. *Nanoscale Horiz.* **2025**, *10*, 2411–2421.
25. Liu, Y.; Zhang, X.; Wang, Y.; Guo, M.; Sheng, J.; Wang, Y.; Wu, T. Promoting neurite outgrowth and neural stem cell migration using aligned nanofibers decorated with protrusions and galectin-1 coating. *Chem. Commun.* **2023**, *59*, 10753–10756.
26. Wang, X.; Xu, Q.; Xu, Y.; Yuan, L.; Guan, X.; Ma, S.; Zhang, D.; Liu, X.; Li, J.; Zhang, T.; et al. Portable absorbable electrical stimulation system for enhanced peripheral nerve repair. *Adv. Funct. Mater.* **2025**, *35*, 2417839.
27. Yi, Z.; Lin, Y.; Jing, R.; Feng, X.; Lu, X.; Tian, D.; Lin, H.; Zhao, L. Dual biomimetic nanofiber conduits enable synergistic NGF delivery and endogenous piezoelectric stimulation for peripheral nerve regeneration. *Adv. Fiber Mater.* **2026**, *8*, 338–358.

28. Guan, W.; Liu, Y.; Jia, M.; Wang, L.; Gao, H.; Sun, S.; Shang, Y.; Shen, H.; Yang, J.; Jin, N.; et al. Magnetic-topological multistage synergy: Anisotropic ovalbumin scaffolds loaded with magnetically-responsive neural cells for long-distance peripheral nerve regeneration. *Bioact. Mater.* **2026**, *57*, 36–53.
29. Zhang, J.; Li, F.; Gao, X.; Qiu, W.; Xia, B.; He, S.; Zhang, Y.; Huang, X.; Liu, B.; Huang, J.; et al. Bamboo-inspired composite conduit accelerates peripheral nerve regeneration through synergistic oriented structure and piezoelectricity. *Adv. Mater.* **2026**, *38*, e09425.
30. Zhang, N.; Yao, X.; Zhang, Q.; Zhang, C.; Zheng, Q.; Wang, Y.; Shan, F. Electrical stimulation promotes peripheral nerve regeneration by upregulating glycolysis and oxidative phosphorylation. *Biochim. Biophys. Acta Mol. Basis Dis.* **2025**, *1871*, 167804.
31. Yan, X.; Liu, J.; Huang, J.; Huang, M.; He, F.; Ye, Z.; Xiao, W.; Hu, X.; Luo, Z. Electrical stimulation induces calcium-dependent neurite outgrowth and immediate early genes expressions of dorsal root ganglion neurons. *Neurochem. Res.* **2014**, *39*, 129–141.
32. Yuan, L.; Zhu, Y.; Li, J.; Jiang, C.; Xu, Q.; Wang, X.; Liu, X.; Wang, X.; Zhang, A.; Zhang, T.; et al. Mesenchymal stem cell-driven neurotrophic bioelectronic platform (MSC-NBP) potentiated peripheral nerve regeneration. *Adv. Funct. Mater.* **2025**, *36*, e23049.
33. Yang, Y.; Yin, X.; Wang, H.; Qiu, W.; Li, L.; Li, F.; Shan, Y.; Zhao, Z.; Li, Z.; Guo, J.; et al. Engineering a wirelessly self-powered and electroconductive scaffold to promote peripheral nerve regeneration. *Nano Energ.* **2023**, *107*, 108145.
34. Qin, C.; Yue, Z.; Forster, R.; Chen, J.; Wallace, G. On demand, wireless electrochemical release of brain derived neurotrophic factor. *Electrochem. Commun.* **2023**, *157*, 107626.
35. Huang, Y.; Jing, W.; Li, Y.; Cai, Q.; Yang, X. Composites made of polyorganophosphazene and carbon nanotube up-regulating osteogenic activity of BMSCs under electrical stimulation. *Colloids Surf. B Biointerf.* **2021**, *204*, 111785.
36. Cheng, H.; Huang, Y.; Chen, W.; Che, J.; Liu, T.; Na, J.; Wang, R.; Fan, Y. Cyclic strain and electrical co-stimulation improve neural differentiation of marrow-derived mesenchymal stem cells. *Front. Cell Dev. Biol.* **2021**, *9*, 624755.
37. Min, G.; Peng, Y.; Wang, W.; Wang, T.; Zhang, Y.; Yin, Z.; Lv, F.; Dong, X.; Xu, S.; Xu, K. Biodegradable dual-stimuli hydrogel scaffoldoid synergizing piezoionic and lithium-ion release for critical-sized bone defect regeneration. *Adv. Funct. Mater.* **2025**, *36*, 2515477.
38. Han, Z.; Wang, F.; Xiong, W.; Meng, C.; Yao, Y.; Cui, W.; Zhang, M. Precise cell type electrical stimulation therapy via force-electric hydrogel microspheres for cartilage healing. *Adv. Mater.* **2025**, *37*, e2414555.
39. Soltani, A.; Azimzadeh, A.; Behboodi, S.; Mamdoohi, M.; Kajbafzadeh, A.-M.; Slavin, K.; Rahimi-Movaghar, V.; Hassannejad, Z. Electrical stimulation enhances sciatic nerve regeneration using a silk-based conductive scaffold beyond traditional nerve guide conduits. *Sci. Rep.* **2024**, *14*, 15196.
40. Greasley, S.; Page, S.; Sirovica, S.; Chen, S.; Martin, R.; Riveiro, A.; Hanna, J.; Porter, A.; Jones, J. Controlling particle size in the stöber process and incorporation of calcium. *J. Colloid Interf. Sci.* **2016**, *469*, 213–223.
41. Stöber, W.; Fink, A.; Bohn, E. Controlled growth of monodisperse silica spheres in the micron size range. *J. Colloid Interf. Sci.* **1968**, *26*, 62–69.
42. Wu, T.; Xue, J.; Xia, Y. Engraving the surface of electrospun microfibers with nanoscale grooves promotes the outgrowth of neurites and the migration of schwann cells. *Angew. Chem. Int. Ed. Engl.* **2020**, *59*, 15626–15632.
43. Parisi, G.; Szewczyk, P.; Narayan, S.; Ura, D.; Knapczyk-Korczak, J.; Stachewicz, U. Multifunctional piezoelectric yarns and meshes for efficient fog water collection, energy harvesting and sensing. *Small Sci.* **2024**, *4*, 00021.
44. Parisi, G.; Szewczyk, P.; Narayan, S. Photoresponsive electrospun fiber meshes with switchable wettability for effective fog water harvesting in variable humidity conditions. *ACS Appl. Mater. Interfaces* **2023**, *33*, 15.
45. Huang, J.; Li, J.; Li, S.; Yang, X.; Huo, N.; Chen, Q.; Wang, W.; Yang, N.; Wang, Y.; Zhou, N. Netrin-1-engineered endothelial cell exosomes induce the formation of pre-regenerative niche to accelerate peripheral nerve repair. *Sci. Adv.* **2024**, *10*, eadm8454.
46. Dutta, K.; Saikia, A.; Singh, A. Transforming lignin into polymer film with improved physiochemical properties by modification with itaconic acid and grafting with polycaprolactone. *Int. J. Biol. Macromol.* **2025**, *305*, 141226.
47. Hyde, E.; Moreno-Atanasio, R.; Neville, F. Fabrication of magnetic core PEI-silica shell particles. *Mater. Res. Bull.* **2017**, *96*, 222–232.
48. Sundaram, V.; Schütza, V.; Schröter, N.; Backhaus, A.; Bilsing, A.; Joneck, L.; Seelbach, A.; Mutschler, C.; Gomez-Sanchez, J.; Schäffner, E.; et al. Adipo-glial signaling mediates metabolic adaptation in peripheral nerve regeneration. *Cell Metab.* **2023**, *35*, 2136–2152.
49. Guo, J.; Guo, Z.; Huang, Y.; Ma, S.; Yan, B.; Pan, C.; Jiang, Z.; Wang, F.; Zhang, Z.; Da, Y.; et al. Blockage of MLKL prevents myelin damage in experimental diabetic neuropathy. *Proc. Natl. Acad. Sci. USA* **2022**, *119*, e2121552119.
50. Cohen, C.; Popovic, M.; Klooster, J.; Weil, M.; Möbius, W.; Nave, K.; Kole, M. Saltatory conduction along myelinated axons involves a periaxonal nanocircuit. *Cell* **2020**, *180*, 311–322.

51. Joe, H.; Seo, H.; Dolkas, J.; Jawala, M.; Hullugundi, S.; Chung, Y.; Patel, H.; Chernov, A.; Shubayev, V. TIMP-1 associates with myelin membrane and preserves myelin in injured peripheral nerve. *Neurobiol. Dis.* **2025**, *209*, 106892.
52. Egger, R.; Tupikov, Y.; Elmaleh, M.; Katlowitz, K.; Benezra, S.; Picardo, M.; Moll, F.; Kornfeld, J.; Jin, D.; Long, M. Local axonal conduction shapes the spatiotemporal properties of neural sequences. *Cell* **2020**, *183*, 537–548.
53. Sun, Y.; Zhang, H.; Zhang, Y.; Liu, Z.; He, D.; Xu, W.; Li, S.; Zhang, C.; Zhang, Z. Li-Mg-Si bioceramics provide a dynamic immuno-modulatory and repair-supportive microenvironment for peripheral nerve regeneration. *Bioact. Mater.* **2023**, *28*, 227–242.
54. Xiao, L.; Sun, Y.; Liao, L.; Su, X. Response of mesenchymal stem cells to surface topography of scaffolds and the underlying mechanisms. *J. Mater. Chem. B* **2023**, *11*, 2550–2567.
55. Yu, L.; Wu, Q.; Jin, F.; Zhang, Y.; Li, M.; Javanmardi, N.; Zhu, H.; Wang, Y.; Yu, X.; Zhou, G.; et al. Self-sustained biomimetic bioelectronic accelerated metabolic reprogramming of bone regeneration. *Biomaterials* **2026**, *325*, 123572.